RESEARCH ARTICLE

NANO · MICRO small
www.small-journal.com

Metal-Free Polymer-Based Current Collector for High Energy Density Lithium-Metal Batteries

Mintao Wan, Ralph Gilles, Jiri Vacik, Haowen Liu, Nae-Lih Wu, Stefano Passerini, and Dominic Bresser**

The energy density of lithium-metal batteries (LMBs) relies substantially on the thickness of the lithium-metal anode. However, a bare, thin lithium foil electrode is vulnerable to fragmentation due to the inhomogeneity of the lithium stripping/plating process, disrupting the electron conduction pathway along the electrode. Accordingly, the current collector is an integral part to prevent the resulting loss of electronic conductivity. However, the common use of a heavy and lithiophobic Cu current collector results in a great anode mass increase and unsatisfactory lithium plating behavior, limiting both the achievable specific energy and the cycle life of LMBs. Herein, a metal-free polymer-based current collector is reported that allows for a substantial mass reduction, while simultaneously extending the cycle life of the lithium-metal anode. The specific mass of the ultra-light, 10 µm thick polymer-based current collector is only 1.03 mg cm^{-2}, which is ≈11% of a 10 µm thick copper foil (8.96 mg cm^{-2}). As a result, LMB cells employing this novel current collector provide a specific energy of 448 Wh kg^{-1}, which is almost 18% higher than that of LMBs using the copper current collector (378 Wh kg^{-1}), and a greatly enhanced cycle life owing to a more homogeneous lithium deposition.

1. Introduction

Lithium-ion batteries (LIBs) have enabled the ongoing electrification of the transportation system owing to their high energy and power density in combination with their excellent cycle life.[1–3] However, further improvements are needed to provide even greater driving ranges and/or lighter batteries in order to address the remaining range anxiety of customers.[4] While there is still room for improvement by enhancing the electrode and cell design and developing advanced electrode active materials such as nickel-rich or manganese-rich $LiNi_{1-x-y}Mn_xCo_yO_2$ (NMC) for the positive electrode[5,6] and silicon-based negative electrodes,[7–9] a substantially greater leap forward could be achieved by transitioning from LIBs to lithium-metal batteries (LMBs), i.e., by using metallic lithium at the negative electrode.[10–12] Lithium metal offers a high theoretical specific capacity of 3860 mAh g^{-1} and a very low redox potential of −3.04 V versus the standard hydrogen electrode, rendering it the ultimate choice for high-energy batteries.[13,14] Nonetheless, there are still a few challenges that need to be overcome, including the risk of lithium dendrite formation, which might short-circuit the cell, and the high reactivity with the commonly used electrolytes.[15–18] Moreover, a frequently overlooked aspect is the requirement of a current collector, which significantly impacts the specific energy of the complete battery cell. In fact, to ensure a genuine electrochemical performance enhancement with sufficiently thin lithium foils, as compared to graphite anodes, a mechanically stable and electronically conductive substrate is essential. This

M. Wan, S. Passerini, D. Bresser
Helmholtz Institute Ulm (HIU)
89081 Ulm, Germany
E-mail: stefano.passerini@kit.edu; dominic.bresser@kit.edu
M. Wan, S. Passerini, D. Bresser
Karlsruhe Institute of Technology (KIT)
76021 Karlsruhe, Germany
R. Gilles
Heinz Maier-Leibnitz Zentrum (MLZ)
Technische Universität München
85748 Garching, Germany
The ORCID identification number(s) for the author(s) of this article can be found under https://doi.org/10.1002/smll.202404437

DOI: 10.1002/smll.202404437

J. Vacik
Nuclear Physics Institute
Academy of Sciences of the Czech Republic
Rez 250 68, Czech Republic
H. Liu, N.-L. Wu
Department of Chemical Engineering
National Taiwan University
Taipei 10617, Taiwan
H. Liu, N.-L. Wu
Advanced Research Center for Green Materials Science and Technology
National Taiwan University
Taipei 10617, Taiwan

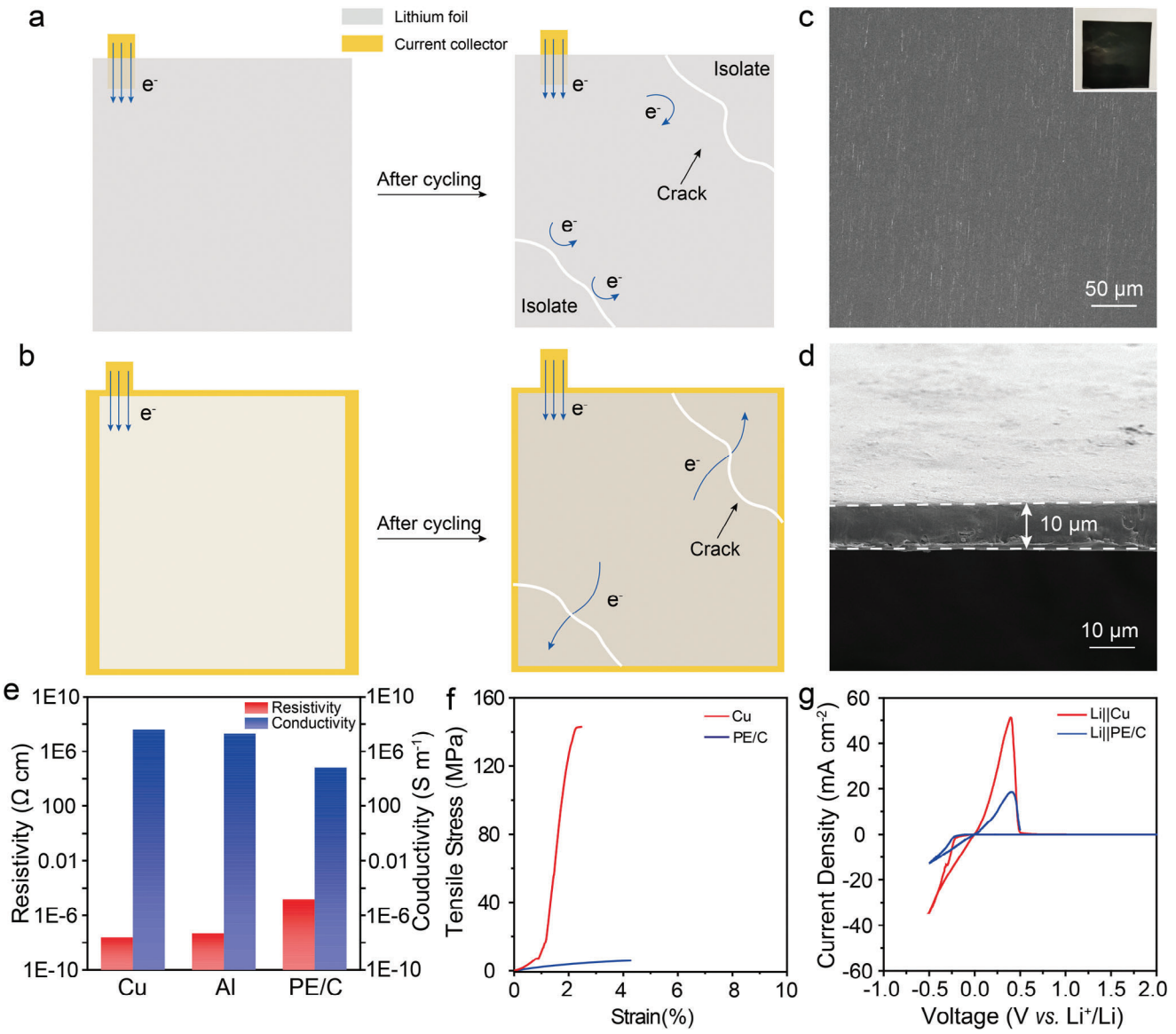

Figure 1. Characterization of the PE/C current collector. a,b) Schematic illustration of the impact of cracks in the lithium foil formed upon continuous cycling in the a) absence and b) presence of a current collector on the electron transport. c,d) SEM micrographs of c) the surface (the inset shows the corresponding photo) and (d) the cross-section of the PE/C current collector. e) Electronic conductivity of the Cu, Al, and PE/C current collector. f) Tensile strength of the Cu and the PE/C current collector. g) Cyclic voltammetry measurements conducted on Li||Cu and the Li||PE/C cells (sweep rate: 10 mV s^{-1}; reversing potentials: −0.5 and 1.0 V vs Li^+/Li).

necessity arises from the inherent softness of metallic lithium[19] and the issue of lithium fragmentation and the consequent loss of electronic conductivity across the electrode, resulting from an inhomogeneous lithium deposition and stripping and the eventual crack formation, as schematically illustrated in **Figure 1**a. In contrast, when a current collector is used, the electrons can still easily migrate across the complete electrode, despite any crack formation, as illustrated in Figure 1b, thus improving the lithium utilization and extending the cycle life compared to bare lithium-metal electrodes without a current collector. Commonly, copper foil is used for this purpose, as it is characterized by its inertness toward metallic lithium (although recent studies have shown that the direct contact between the current collector, lithium, and the electrolyte may result in corrosion issues[20,21]), high electronic conductivity, and facile processability. Moreover, the rather high density of copper (8.96 g cm^{-3}) and the consequent additional mass jeopardizes the potential gain in specific energy,[22,23] especially when thin lithium foils are concerned. Further reducing the lithium thickness results in a further increase of the weight fraction of the current collector and a negligible specific energy increase, but a substantially reduced cycle life owing to the reduced lithium excess (Table S1, Supporting Information). Accordingly, maximizing the potential benefits of the lithium-metal anode with regard to the achievable specific energy drives for a lightweight current collector to replace the heavy copper foil. Recent research on novel current collectors for LIBs includes the

investigation of three-dimensional porous metal foams,[24–26] alternative two-dimensional metal foils,[27–29] various carbon-based current collectors,[30–32] and metal cotaed polymer-based current collectors.[33,34] However, these designs are still facing challenges when used in LMBs due to a myriad of additional issues such as high weight and volume occupation, increased electrolyte consumption, lithiophobic properties, and/or the issue of peeling off in the case of metallic coatings. Thus, the research on novel current collectors for thin lithium-metal anodes necessitates further progress.

In this work, we demonstrated a metal-free current collector for lithium-metal anodes by simply using polyethylene (PE) as the base polymer and carbon nanoparticles (C) as both the conductive matrix and lithiophilic lithium nucleation sites, aiming to enhance both the energy density and lifespan of LMB cells. The resulting PE/C film with a thickness of 10 µm weighed ≈1.03 mg cm^{-2}, i.e., ≈11% of the most commonly used copper current collector with a thickness of 10 µm (8.96 mg cm^{-2}), which dramatically reduces the mass ratio of the electrochemically inactive current collector for the negative electrode. Thus, the specific energy of LMB cells, based on the mass of both the cathode and the anode, including their current collectors, i.e., Al foil and the PE/C film, respectively, could reach ≈448 Wh kg^{-1}. This is ≈18% higher than when using copper as the anode current collector. In addition, due to the lithiophilic properties and the interaction between lithium and carbon, a rather homogeneous lithium-ion deposition and lithium stripping/plating process is achieved on the PE/C current collector, which extends the lifespan of the Li-PE/C||NMC_{622} pouch cell. This lightweight and low-cost conductive polymer appears to be very valuable for the development of high-energy LMBs.

2. Results and Discussion

2.1. Fabrication and Characterization of the PE/C Current Collector

Polyethylene (PE) and carbon black (C) were selected as the base polymer material and the conductive additive, respectively, due to their low cost and abundancy. First, PE powder and carbon black were mixed via ball milling, followed by hot-pressing the mixture at 120 °C. The low-density PE melts at this temperature forming a compact film and embedding the C powder. After cooling to room temperature under pressure, the PE/C polymer film was obtained. To guarantee a uniform thickness, the PE/C composite was hot-calendared to yield films of 6.5 cm by 5 cm (Figure S1, Supporting Information). Furthermore, employing a blow-extrusion technique in industrial settings would offer an even simpler and more cost-effective means of producing the composite PE/C membrane. Fourier-transform infrared (FT-IR) spectra of pure PE and PE/C films show the same peaks located at 2921, 2850, 1463, and 730 cm^{-1} (Figure S2, Supporting Information). X-ray diffraction (XRD) analysis of the PE/C film showed that the PE remained crystalline in this composite to some extent, indicating that the process merely entails a physical blending of the two components (Figure S3, Supporting Information). The scanning electron microscopy (SEM) micrograph shows that the C nanoparticles were evenly distributed in the PE phase, forming a continuous and conductive matrix inside the PE. Unlike previous research on metal-coated polymer-based current collectors, the conductive matrix sealed inside the polymer avoids the risk of conductivity loss caused by the loss of contact between the metal coating and the polymer current collector, and the thickness of the PE/C membrane was determined to be ≈10 µm Figure (1c,d).

The feasible use of the PE/C conductive polymer film as a current collector for lithium-metal anodes was then investigated with regard to the most important properties, including electronic conductivity, electrochemical inertness, and mechanical strength.[33] Four-point probe tests revealed the resistivity of PE/C film to be $1.46 * 10^{-5}$ Ω m, which is substantially higher than that of the Cu current collector ($2.46 * 10^{-8}$ Ω m) and of the Al current collector ($5.74 * 10^{-8}$ Ω m). The high resistivity is not dramatic considering the high conductivity of lithium itself (Figure 1e) and the fact that the PE/C film needs to carry electrons only when and where cracks form in the lithium foil. The tensile strength of the PE/C film, measured using the DMA tension test, is 5.77 MPa, which is not as high as that of the Cu film (142.79 MPa), but higher than that of the Li foil (0.5–1.5 MPa),[35,36] rendering it potentially suitable for the electrode manufacturing (Figure 1f). Additionally, the PE/C film can withstand more than four percent deformation without breaking, displaying the flexibility needed to adjust for non-homogeneities deriving from the continuous plating/stripping process. Finally, the cyclic voltammetry (CV) results obtained for Li||Cu and Li||PE/C cells in the voltage range from −0.5 to 1.0 V (versus Li^+/Li) show similar oxidation and reduction peaks, corresponding to the lithium plating/stripping process (Figure 1g). No other oxidation or reduction peaks were detected in the Li||PE/C cells, proving that no other electrochemical reactions between the PE/C film and metallic lithium or the electrolyte occur, thus, confirming the electrochemical inertness of the PE/C current collector. Considering the above results, it appears that the low-density and low-cost PE/C conductive film is a promising current collector for conductive, but fragile lithium-metal anodes.

2.2. Electrochemical Performance of the PE/C Current Collector

The most prominent advantages of PE/C versus copper are cost and density. The latter is 1.03 g cm^{-3}, i.e., almost 1/9 that of copper with the same thickness (8.96 g cm^{-3}). As shown in **Figure 2**a, the Li-PE/C anode has an areal mass of 3.70 mg cm^{-2}, which is 2.5 times lower than that of the Li-Cu anode with 11.63 mg cm^{-2}. As a result, the PE/C takes only 28% of the total anode mass (i.e., Li-PE/C), while Cu takes ≈77% of the total anode mass (i.e., Li-Cu; Figure 2b). Because of the high mass of Cu, the theoretical specific capacity of the Li-Cu anode is only 886 mAh g^{-1}, i.e., 23% of lithium metal. In contrast, using PE/C results in a theoretical capacity of the Li-PE/C electrode of 2785 mAh g^{-1} (Figure 2c). This is confirmed by the experimental results (Figure 2d–f). The specific capacity of the Li-PE/C electrode was found to be 2623 mAh g^{-1}, which is close to the theoretical value and about thrice higher than that of the Li-Cu electrode with 837 mAh g^{-1}.

To further investigate the electrochemical performance of the Li-PE/C anode for high-energy-density LMBs, bare lithium, Li-Cu, and Li-PE/C, all using 50 µm thick lithium-metal foils, were assembled into pouch cells (Figure S4, Supporting Information) in combination with high mass loading NMC_{622} cathodes

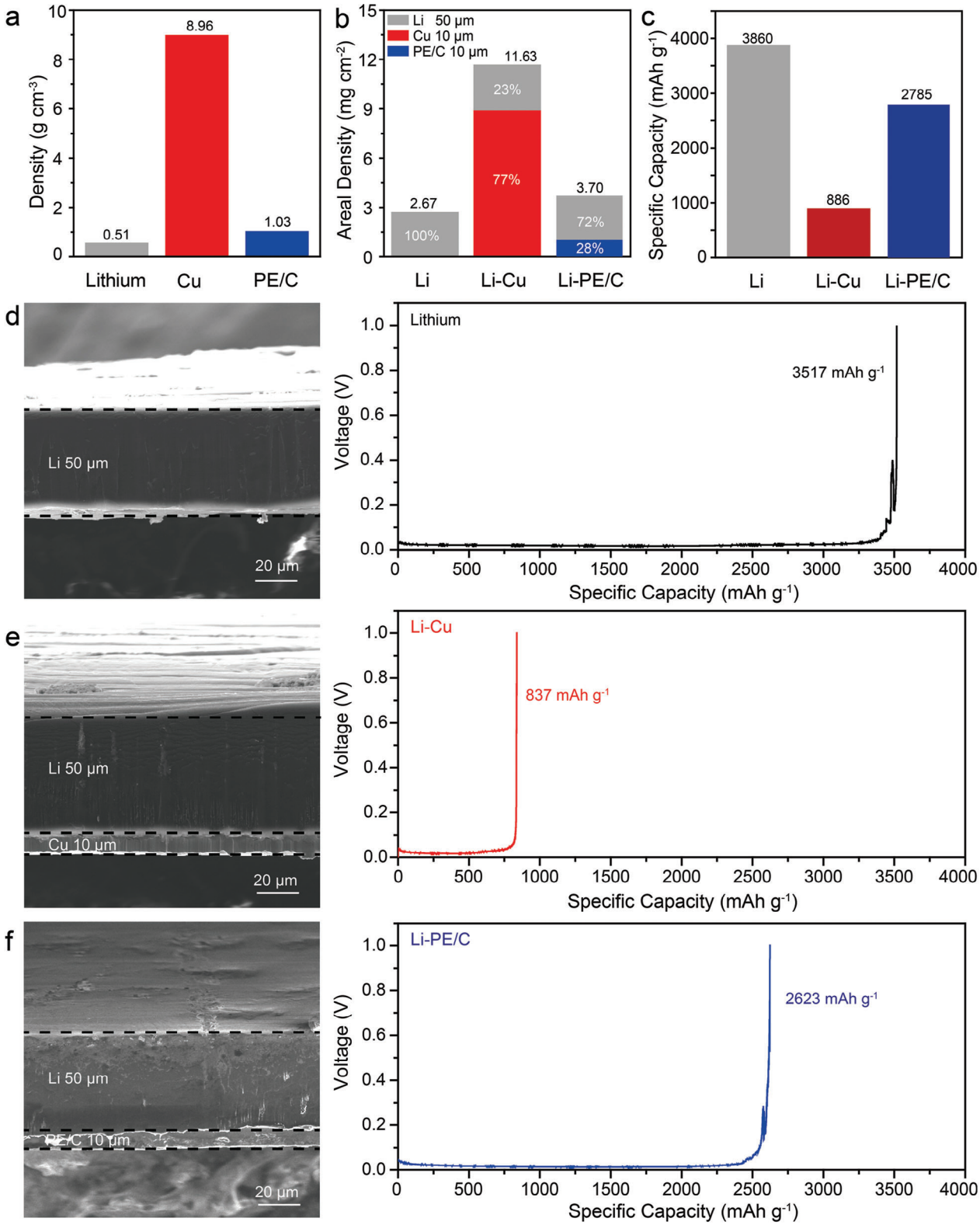

Figure 2. Impact of the mass of the PE/C current collector on the overall specific capacity of the negative electrode. a) Comparison of the density of neat lithium foil, copper foil, and the PE/C foil. b,c) Comparison of the b) areal density and c) theoretical specific capacity of the neat lithium-metal anode, the Li-Cu anode, and the Li-PE/C anode (in all cases, the lithium foil/layer has a thickness of 50 µm). d–f) Cross-sectional SEM micrographs (left) and the experimentally determined specific capacity (right) of d) the neat lithium-metal anode, e) the Li-Cu anode, and f) the Li-PE/C anode; the specific capacity values refer to the mass of the complete negative electrode, i.e., including the mass of the current collector in the case of Li-Cu and Li-PE/C.

(~24 mg cm^{-2}, ~4.2 mAh cm^{-2}, N/P ratio ~2.4). As shown in **Figure 3**, the Li||NMC_{622}, Li-Cu||NMC_{622}, and Li-PE/C||NMC_{622} cells delivered similar specific capacities of ≈~175 mAh g^{-1} using a CCCV/CC test protocol with a current density of ~2.1 mA cm^{-2} in the voltage range from 2.8 to 4.4 V (vs Li^+/Li). However, the specific capacity and specific energy of the Li||NMC_{622} cell showed sharp fading after only 20 cycles. At the same time, the Coulombic efficiency began to fluctuate wildly. The Li||NMC_{622} full-cell retained only 19.7% of its initial specific energy, decreasing from 468 Wh kg^{-1} in the first cycle to 92 Wh kg^{-1} in the 60th cycle. As seen in Figure 3a (left), the dis-/charge profiles of the Li||NMC_{622} full-cell showed an increasing polarization after 5 cycles, which could explain the recession of the Li||NMC_{622} full-cell performance (Figure 3a, right).

Because of the lower anodic specific capacity, the Li-Cu||NMC_{622} full-cell showed a lower first cycle-specific energy of ≈378 Wh kg^{-1}. However, its Coulombic efficiency was more stable than that of the Li||NMC_{622} cell up to 60 cycles, and its specific energy was still 193 Wh kg^{-1}, with a retention of ≈51% (Figure 3b). This improvement is most likely associated to the presence of the Cu current collector, which ensures a sufficiently high electronic conductivity throughout the anode. Nonetheless, the specific capacity and specific energy of the Li-Cu||NMC_{622} cell decreased rapidly after 65 cycles, most likely because of the depletion of active lithium and the accumulation of "dead lithium" caused by an uneven lithium stripping/plating process.

In distinct contrast, the PE/C current collector granted a first cycle-specific energy of ≈448 Wh kg^{-1} for the Li-PE/C||NMC_{622} cell, which is close to the specific energy found for the Li||NMC_{622} cell (Figure 3c, left). Furthermore, the specific capacity and energy retention of the Li-PE/C||NMC_{622} cell were higher than those of the Li||NMC_{622} cell and the Li-Cu||NMC_{622} cell. In fact, the specific energy of the Li-PE/C||NMC_{622} cell was ≈416 Wh kg^{-1} after 60 cycles, resulting in an energy retention of ≈93%. After the 100th cycle, the cell still delivered 282 Wh kg^{-1} (Figure 3c). The polarization of the Li-PE/C||NMC_{622} cell was always smaller than that of the Li||NMC_{622} and the Li-Cu||NMC_{622} cells, resulting in the best cycling performance.

To understand the reasons for such an improvement in the lithium plating/stripping process, electrochemical impedance spectroscopy (EIS) was performed on Li||NMC_{622}, Li-Cu||NMC_{622}, and Li-PE/C||NMC_{622} cells after the formation cycle and after the 20th cycle (Figure S5, Supporting Information). All the cells showed a similar charge transfer impedance of ≈8 ohms after the 1st cycle, indicating that the lower conductivity of PE/C does not severely affect the resistance of the anode (and the entire cell). However, the charge transfer impedance increased substantially for Li||NMC_{622} (ca. 38 ohms) and Li-Cu||NMC_{622} (ca. 19 ohms) after 20 cycles, while that of the Li-PE/C||NMC_{622} cell only increased to ≈11 ohms. These changes perfectly match with the evolution of the cell polarization observed upon the cycling tests, highlighting the capability of PE/C to reduce the cell polarization and extending the battery cycle life.

Besides, since the conductivity of the electrode would have a great impact on the battery performance at high currents, the rate performance of the Li||NMC_{622}, Li-Cu||NMC_{622}, and Li-PE/C||NMC_{622} cells was investigated, applying dis-/charge rates ranging from 0.5C to 10C (1C = 180 mA g^{-1}; areal capacity of the NMC_{622} cathode: ~1.1 mAh cm^{-2}). As displayed in Figure 3d, all cells delivered similar specific capacities at all C rates (≈183 mAh g^{-1} at 0.5C, 177 mAh g^{-1} at 1C, 170 mAh g^{-1} at 2C, 160 mAh g^{-1} at 5C, and 145 mAh g^{-1} at 10C), demonstrating that the lower electronic conductivity of the PE/C did not affect the rate capability, even at high currents (a dis-/charge rate of 10C corresponds to ≈11 mA cm^{-2}), presumably because of the high electronic conductivity of lithium itself. The voltage-time profiles of these three cells show that all cells reached up to 80% of their capacity within 13.5 min (Figure S6, Supporting Information).

2.3. Lithium Stripping/Plating and Degradation Mechanism

Ex situ SEM was performed to investigate the lithium plating behavior on the bare Cu foil and on the PE/C current collector. The lithium deposition process involved two steps, i.e., the lithium nucleation and the lithium growth processes. First, a tiny amount of lithium of 0.01 mAh cm^{-2} was deposited on the Cu foil and on the PE/C film at a current density of 1.0 mA cm^{-2} to investigate the lithium nucleation process. The observed distribution of lithium nuclei on Cu showed the typical aggregative behavior (**Figure 4a**), corresponding to the Volmer-Weber growth mode, which describes the metal deposition situation when the metal-to-metal interaction of the deposited phase is stronger than the metal-to-substrate interaction.[37] Accordingly, metallic lithium preferred to be plated on the previously deposited lithium rather than on the Cu foil and congregated, leaving the majority of the Cu surface free of deposits. A detailed investigation of the lithium clusters revealed that short and thin lithium rods had already formed, even though only 0.01 mAh cm^{-2} metallic lithium was deposited (Figure S7, Supporting Information). After that, more lithium (0.1 mAh cm^{-2}) was plated on the Cu current collector, resulting in the formation of lithium dendrites of various lengths and thicknesses (Figure 4b). During the subsequent lithium stripping process, the elongated lithium dendrites, which might easily break at the root, may form "dead lithium", resulting in poor lithium utilization and low Coulombic efficiency.[17,38] In addition, even after the additional deposition of 4.0 mAh cm^{-2} of lithium on the Cu current collector, still some bare Cu surface is observed in the SEM micrograph (Figure 4e). Indeed, the EDX mapping of the Cu surface after the deposition of 1.0 mAh cm^{-2} of lithium shows an uneven and strong signal of Cu (Figure 4f). Apparently, the aggregative deposition of lithium nuclei on the Cu current collector causes a localized protrusion of porous lithium on the Cu surface and, consequently, an extensive volume expansion of the Li-Cu electrode.

Differently, the SEM micrograph of the PE/C current collector after 0.01 mAh cm^{-2} of lithium plating shows that the metallic lithium was rather randomly distributed, with relatively small nuclei on the PE/C surface (Figure 4g). The further deposition of metallic lithium up to 0.1 mAh cm^{-2} on the PE/C film resulted in the growth of spherical lithium particles, leading to the formation of large globular particles with a size of a few microns, covering the whole current collector surface (Figure 4i,j as well as Figures S8 and S9, Supporting Information). Upon further plating of up to 4.0 mAh cm^{-2}, the lithium deposits merged with each other, resulting in a rather dense structure (Figure 4k). No elongated lithium dendrites were observed on the PE/C current collector surface, supporting for a lower risk of safety hazards

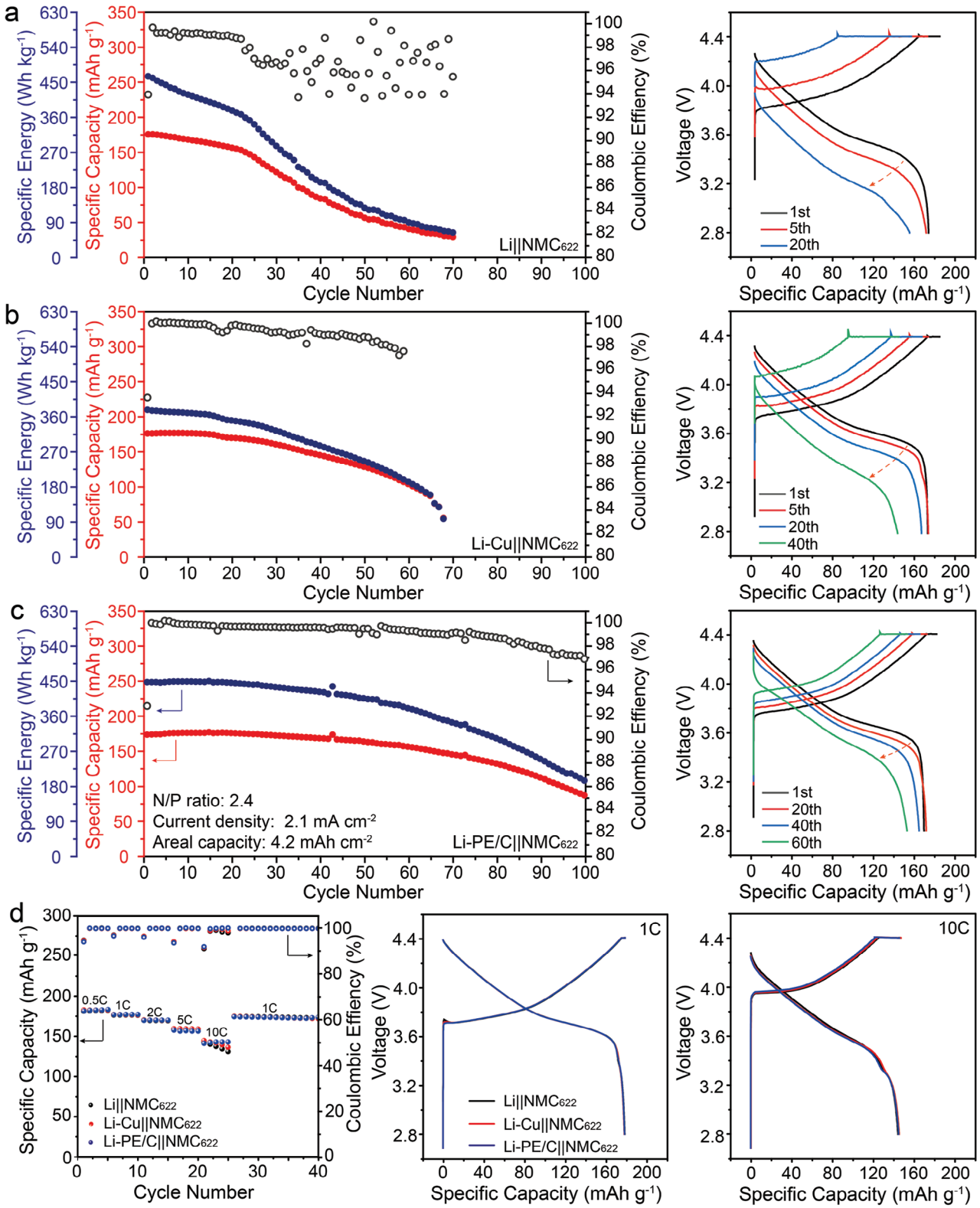

Figure 3. Cycling of LMB full-cells employing an NMC_{622} based cathode. a–c) Plot of the specific capacity, specific energy, and Coulombic efficiency versus the cycle number (left), and selected dis-/charge profiles (right) recorded for the a) Li||NMC_{622}, b) Li-Cu||NMC_{622}, and c)Li-PE/C||NMC_{622} cells (the active material mass loading of the NMC_{622} cathodes was ≈24 mg cm^{-2}). d) Evaluation of the rate capability of the three different cells (left) and exemplary dis-/charge profiles at 1C (middle) and 10C (right) (active material mass loading of the NMC_{622} cathode: 6.5 mg cm^{-2}). All cells were cycled using the CCCV charge/CC discharge test protocol as described in the Experimental Section.

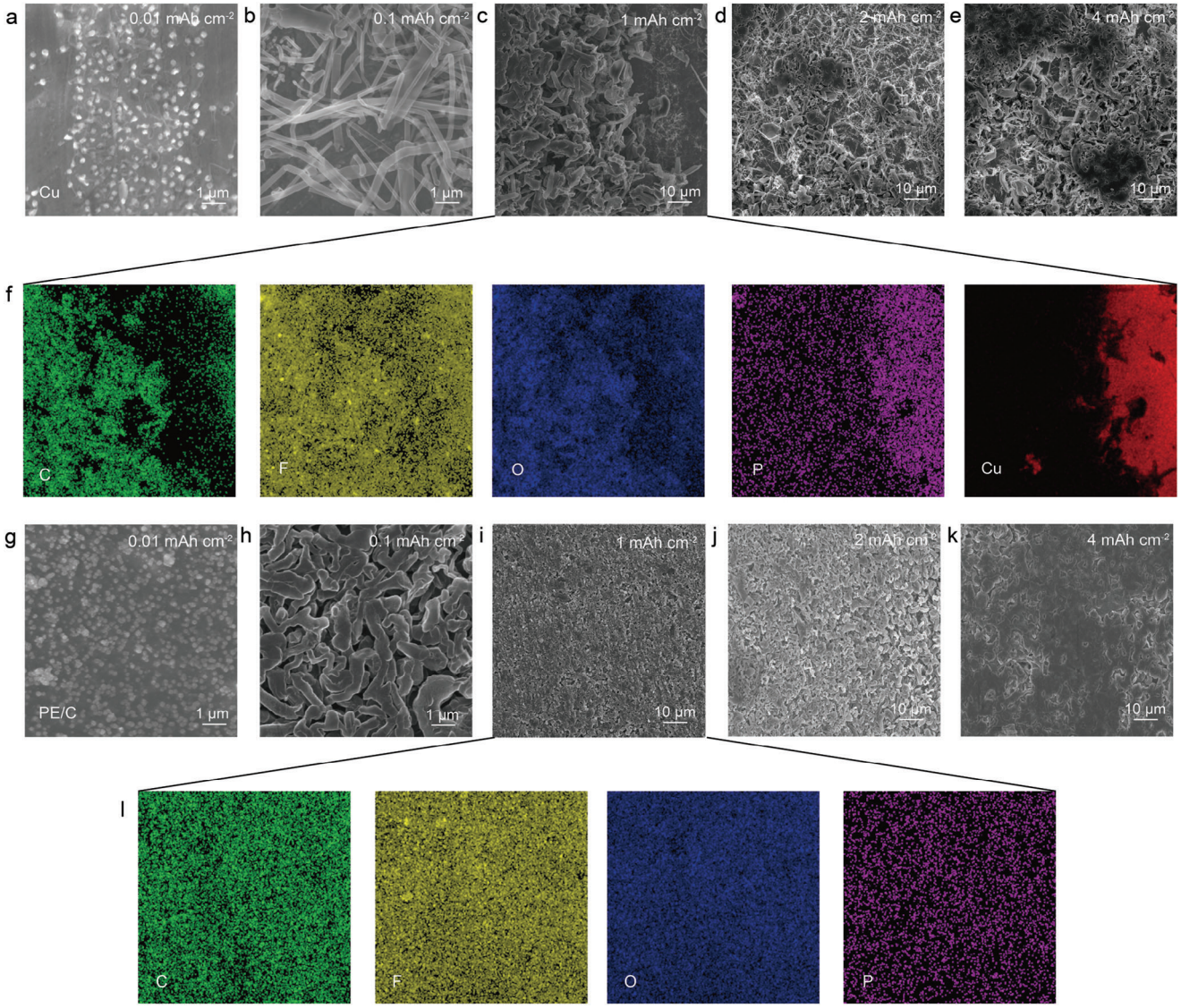

Figure 4. Ex situ SEM/EDX analysis of the Cu and PE/C current collector after lithium plating. a–e) Top-view SEM micrographs of the Cu surface after deposition of a) 0.01 mAh cm^{-2}, b) 0.1 mAh cm^{-2}, c) 1.0 mAh cm^{-2}, d) 2.0 mAh cm^{-2}, and e) 4.0 mAh cm^{-2} of lithium. f) EDX mapping of C, F, O, P, and Cu after depositing 1 mAh cm^{-2} of lithium on the Cu current collector. G,k) Top-view SEM micrographs of the PE/C surface after depositing g) 0.01 mAh cm^{-2}, h) 0.1 mAh cm^{-2}, i) 1.0 mAh cm^{-2}, j) 2.0 mAh cm^{-2}, and k) 4.0 mAh cm^{-2} of lithium. l) EDX mapping of C, F, O, and P after depositing 1.0 mAh cm^{-2} of lithium on the PE/C current collector.

and a reduced formation of "dead lithium." This finding is further corroborated by the determination of a lower exchange current density for the Li||PE/C cell (2.275 mA cm^{-2}) compared to the Li||Cu cell (3.411 mA cm^{-2}), as displayed in Figure S10 (Supporting Information), since a higher exchange current density indicates a preferred lithium deposition on the initially formed lithium nuclei, thus, favoring the growth of dendritic lithium structures.[39,40] The suppressed dendritic lithium growth contributes to the higher (still improvable, though) Coulombic efficiency and longer cycle life of the Li||PE/C cell compared to the Li||Cu cell (Figures S11 and S12, Supporting Information), further evidencing the superiority of the PE/C current collector for a uniform and efficient lithium deposition—even when using a liquid organic carbonate-based electrolyte.

To investigate potential lithium inventory losses due to any interaction between the PE/C current collector and lithium metal, neutron depth profiling (NDP) measurements were conducted. The results indicate a slight accumulation of lithium on the PE/C current collector surface after repeated lithium plating and stripping (**Figure 5**a,b), along with a minor Li gradient into the first ca. 3 µm of the current collector (Figure 5c,d). It appears that this partial lithiation of the evenly distributed C inside the PE/C film (as also evident from the initially lower Coulombic efficiency compared to the Li||Cu cell—see Figure S12, Supporting Information) promotes a homogeneous lithium nucleation process, which turns out favorable for the lithium plating, while the generally small amount of lithium found inside the polymer composite (Figure 5d) and on the back side (Figures S13 and S14,

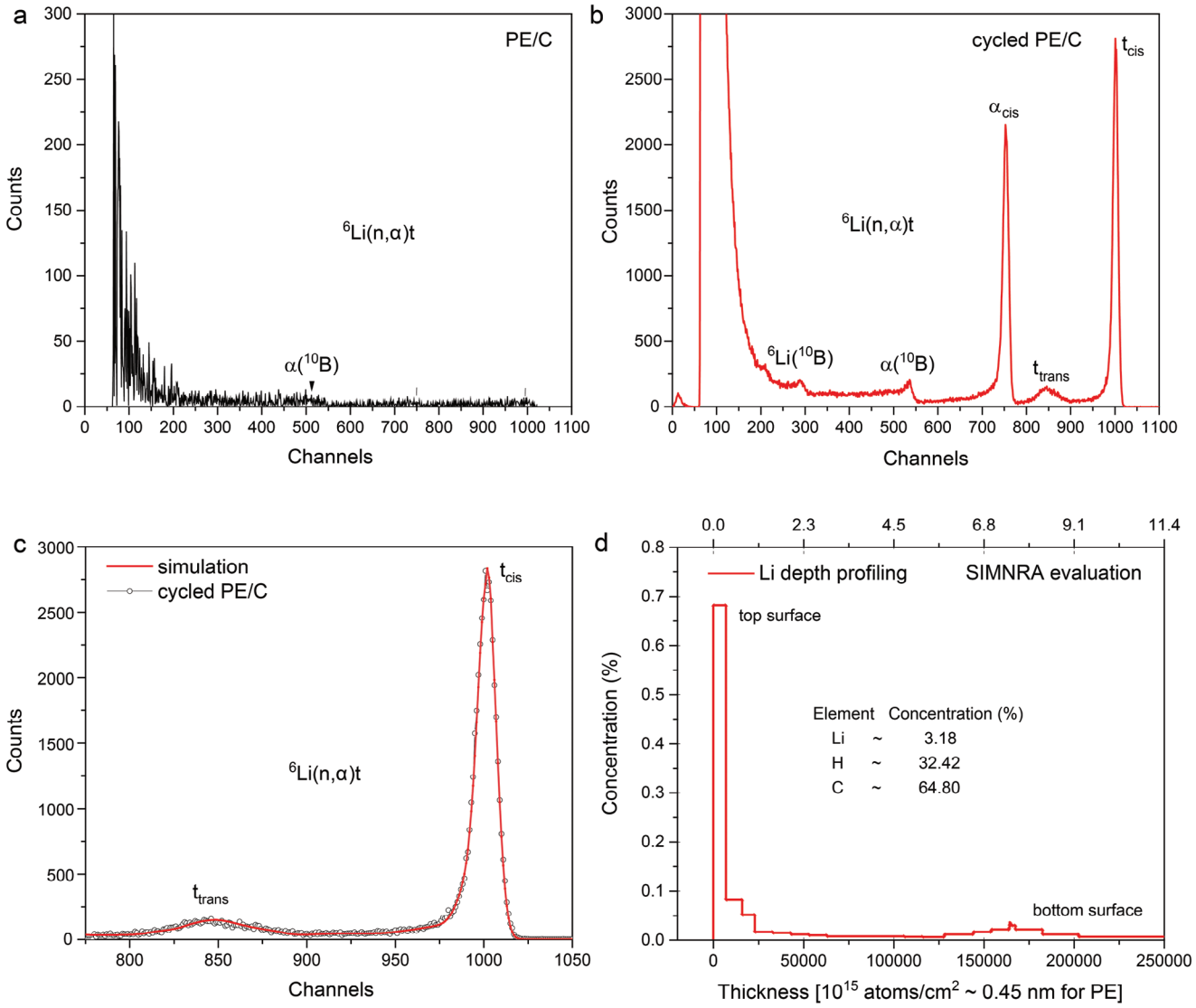

Figure 5. NDP analysis of pristine and cycled PE/C current collectors. a,b) NDP spectrum of a) the pristine PE/C current collector and b) the PE/C current collector after one lithium plating/stripping cycle with a fixed areal capacity of 1.0 mAh cm^{-2} at a current density of 1.0 mA cm^{-2}. c,d) NDP spectrum of ^{6}Li for c) the cycled PE/C current collector, and d) its simulated depth distribution across the PE/C current collector (the sample was studied from the front side).

Supporting Information) of the PE/C current collector (the latter presumably resulting from the lithium salt in the electrolyte) indicates an extremely weak, essentially absent chemical reaction between the polymer-based current collector and lithium.

In sum, the SEM, EDX, and NDP results show that the lithium plating occurs relatively smoothly on the PE/C current collector, which is key for the superior performance of the Li-PE/C anodes in the NMC_{622}-based full-cells. In fact, when cracks occur within the lithium layer upon cycling, areas of the lithium foil get electrochemically "lost" in the absence of an electron-conductive substrate because of the lack of electronic conductivity within the electrode. Even worse, the edge of the active lithium might serve as the onset for dendritic lithium growth in such case (**Figure** 6a). As a matter of fact, the SEM micrograph of the bare Li anode after twenty cycles in Li||NMC_{622} pouch cells shows a large fissure with a width of tens of microns across the entire lithium foil (Figure 6d), which supports the aforementioned reasoning and provides an explanation for the rather poor cycling performance of these cells. This fading mechanism is oppressed in the Li-Cu||NMC_{622} pouch cells, even though also, in this case, some minor cracks formed inside the lithium foil, but the presence of the Cu current collector grants a sufficient electronic conductivity within the electrode and, thus, enables a better cycling stability of the Li-Cu||NMC_{622} cells compared to the Li||NMC_{622} cells. Nonetheless, since in this case, lithium prefers to be deposited on already present lithium rather than on the Cu foil, the Li-Cu anode tends to become porous and its surface uneven upon cycling (Figure 6b). And, indeed, the top-view SEM micrograph of the Li-Cu anode reveals some bare Cu foil, while the morphology of the deposited lithium is rather rough and patchy after twenty cycles

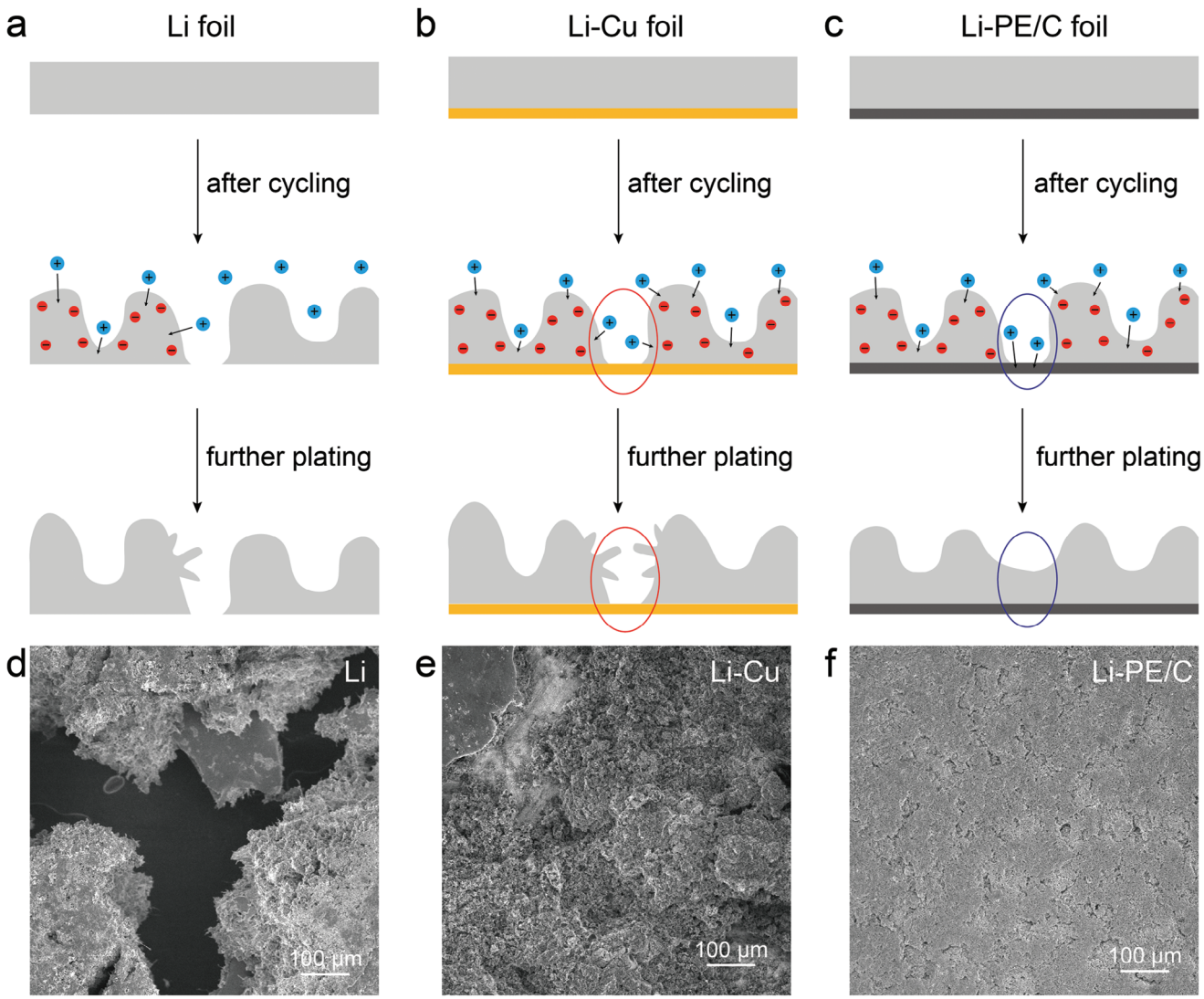

Figure 6. Fading mechanism of the Li-metal negative electrodes. a–c) Schematic illustration of the fading mechanism for the a) Li, b) Li-Cu, and c) Li-PE/C negative electrodes. d–f) Ex situ top-view SEM micrographs of the d) Li, e) Li-Cu, and f) Li-PE/C negative electrodes after 20 cycles in LMB pouch cells employing NMC_{622}-based positive electrodes (mass loading: 24 mg cm^{-2}, N/P ratio: 2.4).

(Figure 6e). In stark contrast, the surface of the Li-PE/C electrode remains very smooth, crack-free and even after 20 cycles, and no bare PE/C surface is observed (Figure 6f), confirming that the lithium deposition on this novel current collector is much more favorable and indicating that any potentially formed cracks or inhomogeneities are filled up with lithium again upon continuous plating and stripping (Figure 6c). Such mechanism explains the enhanced long-term cycling performance of the Li-PE/C||NMC_{622} cells, further highlighting the benefits of such lightweight and cost-efficient current collector.

3. Conclusion

The development of an electronically conductive polymer film comprising two low-cost components, polyethylene (PE) and carbon black (C), via a simple hot-pressing method is demonstrated. The resulting lithiophilic low-density PE/C film provides an alternative current collector for the lithium-metal anode, allowing for the substantial reduction of the cell weight and, thus, a significant increase in specific energy. In addition, the use of the PE/C current collector yields a more homogeneous and denser lithium deposition compared to the commonly employed copper current collector. As a result, the Li-PE/C||NMC_{622} cells provide a longer cycle life than the Li||NMC_{622} or Li-Cu||NMC_{622} cells, while offering higher specific energy of 448 Wh kg^{-1} compared to the Li-Cu||NMC_{622} cells (378 Wh kg^{-1}), close to that of the Li||NMC_{622} cells, which show the worst cycling stability. This novel PE/C current collector is particularly attractive for commercial use as it promises a significant cost reduction compared to metallic copper. Hence, we may anticipate that the results reported herein are not only shedding light on a commonly overlooked, though fundamentally important challenge, but moreover, provide a new avenue for the development of cost-competitive, high-performance LMBs.

4. Experimental Section

Preparation of the PE/C Current Collector: 3.5 g polyethylene (PE) and 1.5 g carbon black (C) were mixed via ball milling at 400 rpm for 4 h. This composition provides sufficient electronic conductivity, while still allowing for the realization of easily processable PE/C membranes. Subsequently, the mixture was pressed at 200 t and 120 °C, i.e., slightly above the melting temperature of polyethylene (117 °C), to yield a compact, non-porous film. Finally, the film was hot-calendared (120 °C) to obtain a uniform thickness of 10 µm.

Basic Characterization: The composition and morphology of the PE/C conductive polymer films were investigated via Fourier-transform infrared (FT-IR) spectroscopy (Bruker VERTEX 70v), X-ray diffraction (XRD, Bruker D8 Advance diffractometer), and scanning electron microscopy (SEM; ZEISS EVO MA 10 microscope). The conductivity of the Cu, Al, and PE/C current collector was determined using a Jandel CYL-RM3000 four-point probe system. The tensile strength was determined by dynamic mechanical analysis (DMA; Q800, TA Instruments, Inc.). Each sample was measured using an isotactic force test with a force ramp rate of 1 N min^{-1} at 25 °C until the maximum of 18 N was reached or until the sample broke. The ex situ SEM analysis of the current collectors was performed by disassembling the cells in an argon-filed glovebox (MBraun, O_2 and H_2O content of <0.1 ppm) and rinsing the samples with dimethyl carbonate (DMC) to remove any residual electrolyte before transferring them into the SEM using an airtight transfer box.

Electrochemical Testing: 2032 coin-type Li||Cu, Li||PE/C cells (Hohsen) were assembled in an argon-filled glove box (MBraun, O_2 and H_2O content of <0.1 ppm). Cyclic voltammetry (CV) measurements for the Li||Cu and Li||PE/C cells were performed using a Biologic VMP system in the voltage range from −0.5 to 2.0 V with a sweep rate of 10 mV s^{-1}.

The Li||NMC_{622}, Li-Cu||NMC_{622}, and Li-PE/C||NMC_{622} pouch cells were assembled in a dry room with a dew point below −70 °C. The lithium foil (Honjo) had a thickness of 50 µm, equivalent to ≈10 mAh cm^{-2}. The positive electrodes based on $LiNi_{0.6}Mn_{0.2}Co_{0.2}O_2$ (NMC_{622}, BASF) as the active material had a mass loading of either 24 mg cm^{-2} (i.e., 4.2 mAh cm^{-2}) for the constant current cycling tests or 6.5 mg cm^{-2} (i.e., 1.1 mAh cm^{-2}) for the rate capability studies. Both kinds of NMC_{622} cathodes were fabricated comprising 90 wt.% NMC_{622}, 5 wt.% polyvinylidene fluoride (PVdF, Solvay, Solef 6020), and 5% carbon black (Super C_{65}, IMERYS). 1 M $LiPF_6$, dissolved in a 4:1 volume mixture of DMC and fluoroethylene carbonate (FEC) served as the electrolyte. All components were purchased from Sigma–Aldrich. A sheet of Celgard 2500 with a thickness of 25 µm was utilized as the separator in all cases. The cycling performance of the high mass loading cells was investigated applying a "constant current charge-constant voltage/constant current discharge (CCCV/CC)" mode in the voltage range from 2.8 to 4.4 V with a dis-/charge rate of 0.5C (2.1 mA cm^{-2}, 1C = 180 mA g^{-1}). When the voltage reached 4.4 V, a constant voltage charge process (4.4 V) was applied until the charge current decayed to 0.02C. Electrochemical impedance spectroscopy (EIS) was conducted for these cells after the 1st and 20th cycle in the discharged state using a Biologic VMP and applying a frequency range from 100 kHz to 100 mHz with a voltage amplitude of 10 mV. The rate performance tests of low mass loading NMC_{622} cells were also performed using the CCCV/CC protocol in the voltage range from 2.8 to 4.4 V at 0.5, 1, 2, 5, and 10 C (1C = 180 mA g^{-1}) with the CV step being limited to 0.02C. All the cycling performance and rate capability testing were conducted on a Maccor 4000 battery test equipment.

The Coulombic efficiency of the Li||Cu and Li||PE/C cells was investigated in a galvanostatic mode at a current density of 1.0 mA cm^{-2} and capacity of 1.0 mAh cm^{-2}. The Tafel plots of Li||Cu and Li||PE/C cells were obtained by linear sweep voltammetry (LSV) measurements using a Biologic VMP system in the voltage range from 0.2 to −0.2 V (vs Li^+/Li) with a sweep rate of 10 mV s^{-1}. All the cells mentioned above were studied at 20 °C.

Neutron Depth Profiling: The depth distribution of Li was measured using the nondestructive neutron depth profiling (NDP). NDP was based on the measurement and analysis of residual energies of the alpha and triton reaction products that are isotropically emitted from the $^6Li(n_{th},\alpha)t$ nuclear reaction induced by thermal neutrons. Although the natural abundance of ^6Li is only ≈7.6%, the high cross section (σ = 940 b) and the high energy of reaction (Q = 4785 keV) allow for the depth distribution of Li in solids to be measured with high sensitivity. The measurement of the samples was carried out on the NDP spectrometer of the NPI CANAM infrastructure at the nuclear research reactor LVR15 (operated by the Research Center Rez). The spectrometer, installed on a short supermirror neutron-guide, uses a well thermalized neutron beam with a relatively high flux of 6×10^7 n_{th} cm^{-2} s^{-1}. The spectrometer includes a multipurpose vacuum chamber with different detection systems with fully and partially depleted solid-state detectors, as well as multi-pixel detectors, which allows different detection modes with a single-state detector or with two detectors (in coincidence measurement, which is, however, suitable only for thin samples with a thickness of a few micrometers). In this experiment, the samples were analyzed using fully-depleted Canberra-type detectors with a sensitive area of 50 mm^2. The detector-sample distance was 55 mm, and the solid angle was set to 2×10^{-3} rad. In this experimental setup, the counting rate of the reaction products for the measured Li-PE/C sample was a few counts per second. The energy resolution of the spectrometer was ≈2.5 keV per channel. During the measurements, the NDP chamber was evacuated to the level of 10^{-1} mbar (due to the short path between the detector and the sample, the energy loss of the reaction products at 0.1 mbar was negligible). Special interactive codes including SIMNRA were used in this experiment to evaluate the NDP spectra.

Supporting Information

Supporting Information is available from the Wiley Online Library or from the author.

Acknowledgements

The authors would like to acknowledge financial support from the Helmholtz Association and the German Federal Ministry of Education and Research (BMBF) within the ExcellBattUlm project (03XP0257D), the ExZellTUM III project (03XP0255), and the HighSafe-3 project (03XP0568A). The NDP measurements were carried out at the infrastructures "CANAM" and 'Reactors LVR-15 and LR-0′ supported by the Ministry of Education, Youth and Sports of the Czech Republic.

Open access funding enabled and organized by Projekt DEAL.

Conflict of Interest

The authors declare no conflict of interest.

Data Availability Statement

The data that support the findings of this study are available from the corresponding author upon reasonable request.

Keywords

anode, battery, current collector, lithium metal, polymer

Received: May 31, 2024
Revised: August 25, 2024
Published online:

[1] M. Armand, J. M. Tarascon, *Nature* **2008**, *451*, 652.

[2] M. Marinaro, D. Bresser, E. Beyer, P. Faguy, K. Hosoi, H. Li, J. Sakovica, K. Amine, M. Wohlfahrt-Mehrens, S. Passerini, *J. Power Sources* **2020**, *459*, 228073.
[3] M. Armand, P. Axmann, D. Bresser, M. Copley, K. Edström, C. Ekberg, D. Guyomard, B. Lestriez, P. Novák, M. Petranikova, W. Porcher, S. Trabesinger, M. Wohlfahrt-Mehrens, H. Zhang, *J. Power Sources* **2020**, *479*, 228708.
[4] S. Chu, Y. Cui, N. Liu, *Nat. Mater.* **2017**, *16*, 16.
[5] A. Gomez-Martin, F. Reissig, L. Frankenstein, M. Heidbüchel, M. Winter, T. Placke, R. Schmuch, *Adv. Energy Mater.* **2022**, *12*, 2103045.
[6] W. D. Li, S. Lee, A. Manthiram, *Adv. Mater.* **2020**, *32*, 2002718.
[7] J. Chen, X. L. Fan, Q. Li, H. B. Yang, M. R. Khoshi, Y. B. Xu, S. Hwang, L. Chen, X. Ji, C. Y. Yang, H. X. He, C. M. Wang, E. Garfunkel, D. Su, O. Borodin, C. S. Wang, *Nat. Energy* **2020**, *5*, 386.
[8] P. Li, H. Kim, S. T. Myung, Y. K. Sun, *Energy Storage Mater.* **2021**, *35*, 550.
[9] M. Ko, S. Chae, J. Ma, N. Kim, H.-W. Lee, Y. Cui, J. Cho, *Nat. Energy* **2016**, *1*, 16113.
[10] J. Liu, Z. N. Bao, Y. Cui, E. J. Dufek, J. B. Goodenough, P. Khalifah, Q. Y. Li, B. Y. Liaw, P. Liu, A. Manthiram, Y. S. Meng, V. R. Subramanian, M. F. Toney, V. V. Viswanathan, M. S. Whittingham, J. Xiao, W. Xu, J. H. Yang, X. Q. Yang, J. G. Zhang, *Nat. Energy* **2019**, *4*, 180.
[11] Y. Qiao, H. Deng, P. He, H. S. Zhou, *Joule* **2020**, *4*, 1445.
[12] C. J. Niu, H. Lee, S. R. Chen, Q. Y. Li, J. Du, W. Xu, J. G. Zhang, M. S. Whittingham, J. Xiao, J. Liu, *Nat. Energy* **2019**, *4*, 551.
[13] J. M. Tarascon, M. Armand, *Nature* **2001**, *414*, 359.
[14] W. Xu, J. Wang, F. Ding, X. Chen, E. Nasybutin, Y. Zhang, J.-G. Zhang, *Energy Environ. Sci.* **2014**, *7*, 513.
[15] D. Lin, Y. Liu, Y. Cui, *Nat. Nanotechnol.* **2017**, *12*, 194.
[16] J. Xiao, *Science* **2019**, *366*, 426.
[17] C. C. Fang, J. X. Li, M. H. Zhang, Y. H. Zhang, F. Yang, J. Z. Lee, M. H. Lee, J. Alvarado, M. A. Schroeder, Y. Y. C. Yang, B. Y. Lu, N. Williams, M. Ceja, L. Yang, M. Cai, J. Gu, K. Xu, X. F. Wang, Y. S. Meng, *Nature* **2019**, *572*, 511.
[18] X. He, D. Bresser, S. Passerini, F. Baakes, U. Krewer, J. Lopez, C. T. Mallia, Y. Shao-Horn, I. Cekic-Laskovic, S. Wiemers-Meyer, F. A. Soto, V. Ponce, J. M. Seminario, P. B. Balbuena, H. Jia, W. Xu, Y. B. Xu, C. M. Wang, B. Horstmann, R. Amine, C. C. Su, J. Y. Shi, K. Amine, M. Winter, A. Latz, R. Kostecki, *Nat. Rev. Mater.* **2021**, *6*, 1036.
[19] W. Wu, W. Luo, Y. Huang, *Chem. Soc. Rev.* **2023**, *52*, 2553.
[20] J. F. Dohmann, F. Horsthemke, V. Küpers, S. Bloch, Y. Preibisch, A. Kolesnikov, M. Kolek, M. C. Stan, M. Winter, P. Bieker, *Adv. Energy Mater.* **2021**, *11*, 2101021.
[21] A. Kolesnikov, M. Kolek, J. F. Dohmann, F. Horsthemke, M. Boerner, P. Bieker, M. Winter, M. C. Stan, *Adv. Energy Mater.* **2020**, *10*, 2000017.
[22] C. Niu, D. Liu, J. A. Lochala, C. S. Anderson, X. Cao, M. E. Gross, W. Xu, J.-G. Zhang, M. S. Whittingham, J. Xiao, J. Liu, *Nat. Energy* **2021**, *6*, 723.
[23] D. Wang, J. Qiu, N. Inui, R. Hagiwara, J. Hwang, K. Matsumoto, *ACS Energy Lett.* **2023**, *8*, 5248.
[24] Y. Q. Li, J. C. Li, X. Y. Lang, Z. Wen, W. T. Zheng, Q. Jiang, *Adv. Funct. Mater.* **2017**, *27*, 1700447.
[25] B. Liu, J. Zhang, X. F. Wang, G. Chen, D. Chen, C. W. Zhou, G. Z. Shen, *Nano Lett.* **2012**, *12*, 3005.
[26] L. Fu, M. T. Wan, B. Zhang, Y. F. Yuan, Y. Jin, W. Y. Wang, X. C. Wang, Y. J. Li, L. Wang, J. J. Jiang, J. Lu, Y. M. Sun, *Adv. Mater.* **2020**, *32*, 2000952.
[27] V. Pande, V. Viswanathan, *ACS Energy Lett.* **2019**, *4*, 2952.
[28] S. T. Wang, K. V. Kravchyk, A. N. Filippin, U. Muller, A. N. Tiwari, S. Buecheler, M. I. Bodnarchuk, M. V. Kovalenko, *Adv. Sci.* **2018**, *5*, 1700712.
[29] Y. Gu, H. Y. Xu, X. G. Zhang, W. W. Wang, J. W. He, S. Tang, J. W. Yan, D. Y. Wu, M. S. Zheng, Q. F. Dong, B. W. Mao, *Angew. Chem., Int. Ed.* **2019**, *58*, 3092.
[30] H. Kwon, J.-H. Lee, Y. Roh, J. Baek, D. J. Shin, J. K. Yoon, H. J. Ha, J. Y. Kim, H.-T. Kim, *Nat. Commun.* **2021**, *12*, 5537.
[31] L. Liu, Y.-X. Yin, J.-Y. Li, S.-H. Wang, Y.-G. Guo, L.-J. Wan, *Adv. Mater.* **2018**, *8*, 1706216,
[32] D. Lin, Y. Liu, Z. Liang, H.-W. Lee, J. Sun, H. Wang, K. Yan, J. Xie, Y. Cui, *Nat. Nanotechnol.* **2016**, *11*, 626.
[33] Y. Ye, L.-Y. Chou, Y. Liu, H. Wang, H. K. Lee, W. Huang, J. Wan, K. Liu, G. Zhou, Y. Yang, A. Yang, X. Xiao, X. Gao, D. T. Boyle, H. Chen, W. Zhang, S. C. Kim, Y. Cui, *Nat. Energy* **2020**, *5*, 786.
[34] C. H. Zhang, Y. J. Guo, S. J. Tan, Y. H. Wang, J. C. Guo, Y. F. Tian, X. S. Zhang, B. Z. Liu, S. Xin, J. Zhang, L. J. Wan, Y. G. Guo, *Sci. Adv.* **2024**, *10*, 11.
[35] C. D. Fincher, D. Ojeda, Y. Zhang, G. M. Pharr, M. Pharr, *Acta Mater.* **2020**, *186*, 215.
[36] J. C. Stallard, S. Vema, C. P. Grey, V. S. Deshpande, N. A. Fleck, *Acta Mater.* **2023**, *260*, 119313.
[37] R. Koch, D. Hu, A. K. Das, *Phys. Rev. Lett.* **2005**, *94*, 146101.
[38] F. Liu, R. Xu, Y. Wu, D. T. Boyle, A. Yang, J. Xu, Y. Zhu, Y. Ye, Z. Yu, Z. Zhang, X. Xiao, W. Huang, H. Wang, H. Chen, Y. Cui, *Nature* **2021**, *600*, 659.
[39] Y. Y. Liu, X. Y. Xu, M. Sadd, O. O. Kapitanova, V. A. Krivchenko, J. Ban, J. L. Wang, X. X. Jiao, Z. X. Song, J. X. Song, S. Z. Xiong, A. Matic, *Adv. Sci.* **2021**, *8*, 2003301.
[40] J. Lopez, A. Pei, J. Y. Oh, G. J. N. Wang, Y. Cui, Z. A. Bao, *J. Am. Chem. Soc.* **2018**, *140*, 11735.